PANAMGEO CHILE 2024
17th PAN-AMERICAN CONFERENCE ON SOIL MECHANICS AND GEOTECHNICAL ENGINEERING | 2nd LATIN-AMERICAN REGIONAL CONFERENCE OF IAEG
LA SERENA • CHILE / NOVEMBER 12 - 16, 2024

Proceedings of the 17th Pan-American Conference on Soil Mechanics and Geotechnical Engineering (XVII PCSMGE), and 2nd Latin-American Regional Conference of the International Association for Engineering Geology and the Environment (IAEG), La Serena Chile, 2024.

Three-dimensional finite element analysis of a pile group under lateral loading

Análisis tridimensional de elementos finitos de un grupo de pilotes cargados lateralmente

Erick Tafur
Carrera de Ingeniería Civil, Universidad de Lima, Perú, 20173930@aloe.ulima.edu.pe

Marko López
Instituto de Investigación Científica, Carrera de Ingeniería Civil, Universidad de Lima, Perú

Roberto Quevedo
Tecgraf Institute at Pontifical Catholic University of Rio de Janeiro, PUC-Rio, Brazil

ABSTRACT: Structures such as high-rise buildings, wind turbines, and transport infrastructure play a crucial role in driving the economic growth of countries. In Peru, construction activities have been on the rise. However, this surge in construction projects is not always matched by improvements in safety standards, which are critical for ensuring the structural integrity and longevity of these projects. Notably, pile groups form effective foundations that allow the application of substantial loads in unfavorable soil conditions. Despite their advantages, the use of pile groups presents significant challenges in engineering, particularly concerning the interactions between piles and the surrounding soil. These challenges become more pronounced under horizontal loads generated by seismic waves and wind forces. Such horizontal loads can lead to a progressive reduction in the resistance and rigidity of soil, reducing its bearing capacity and inducing unacceptable strains that could compromise the stability of structures supported by the soil foundation. In this study, three-dimensional numerical simulations were performed using the finite element method to assess the mechanical behavior of a pile group subjected to vertical, horizontal, and bending moment loads in different soil types. The soil–structure interaction was modeled by combining the Winkler–Spring method with the Matlock and Reese method to determine subgrade moduli at varying depths. In this case, soil was modeled as a deformable element. Comparing the obtained results with those derived from a model considering soil as a rigid material revealed that the current study provides a more precise analysis of pile groups. This study also determined key factors such as shear forces, bending moments, lateral displacements, and safety factors, which are critical for designing foundations adhering to the specifications of the ACI 318-19 standard.

KEYWORDS: ACI 318-19, Geo5, pile group, soil–structure interaction, RFEM.

1. INTRODUCTION

Failures in construction projects are often related to issues in geotechnical analyses and the impacts of large loads such as earthquakes, wind, and waves, which compromise the shear strength and bending capacities of structures (Ballesteros, 2018). This highlights the importance of designing structures with high resistance capacities, considering the lateral forces induced by dynamic events, such as earthquakes. For instance, in 2017, the *El Niño* phenomenon in Peru led to numerous structural and geotechnical issues in several bridges owing to the lack of consideration of horizontal loads in their designs (Cépeda, 2020).

To ensure that structures exhibit adequate efficiency and comply with design criteria related to factors such as load-bearing capacity and settlements, accurate representations of soil properties and soil–structure interactions are crucial. Furthermore, when analyzing axial loads on immersed groups of piles, considerations of horizontal loads, particularly those with substantial magnitudes, are critical for appropriate designs (Kim & Jeong, 2011).

Horizontal loads originate from wind or seismic activities, accounting for approximately 10%–15% of the vertical loads of terrestrial structures. Meanwhile, in maritime areas, wave action can induce horizontal loads, accounting for over 30% of vertical loads (Abdrabbo & Gaaver, 2012). The choice of foundations, particularly involving pile groups, must be based on factors such as the magnitude of the load, load transmission capacity of soil, and thickness and composition of the soil stratum.

Notably, soil–pile interactions are highly complex owing to the mutual dependence of pile deflections and resulting soil reactions (Abdrabbo & Gaaver, 2012). Research into the behaviors of pile groups has led to various modeling approaches. One notable approach simplifies the analysis by replacing the soil around the piles with spring elements. Consequently, pile–pile interactions can be neglected, facilitating a continuous elastic analysis of the system (Rollins et al., 2005).

Alternatively, the method proposed by Stacul and Squeglia (2018) accounts for the nonlinear characteristics of soil using the hyperbolic modulus of the reduction curve within the contour elements method, which is associated with the modified Kovacs methodology for soil modeling. Remarkably, the proposed approach demonstrated improved computational efficiency compared to more sophisticated codes, such as Plaxis 3D. The accuracy of the model was validated through large-scale on-site tests subjecting piles and pile groups to lateral loading. The results of tests on 15 pile groups revealed prediction errors below 30%, demonstrating the accuracy of the model. This accuracy was attributed to the influence of soil pressure resulting from increased surface stiffness and the model's consideration of highly nonlinear soil–structure interactions.

Teramoto et al. (2018) conducted a 3D elastoplastic finite element analysis to analyze the mechanical behavior of a pile group subjected to lateral loads and validated their results with the outcomes of large-scale experimental tests. Their results revealed that the proposed methodology effectively reduced the maximum reaction forces in the subgrade beneath the rear piles, which is critical for structural and geotechnical design. Furthermore, through an analysis of the force distribution, they reported that the front pile experienced the maximum deformation, while the rear piles were subjected to weaker reaction forces owing to the decreasing load distribution across the group.

Thus, accurate analysis and considerations of horizontal loads are critical for precise geotechnical examinations and future designs of foundations. This study aims to examine soil–pile interactions using both linear and nonlinear finite element analyses. The study determines the subgrade modulus, examines the interactions among pile heads and the piles themselves, and assesses the mechanical parameters of the soil. Leveraging a calculation methodology, the study then investigates the effect of the pile diameter on the behavior of the pile group under lateral loads, aiming to optimize operational efficiency and avoid issues such as load overlaps or oversized systems. This approach ensures that appropriate safety factors are derived and incorporated into the design.

2. THEORETICAL FRAMEWORK

2.1. Laterally loaded piles

When a vertical pile is subjected to a lateral load, the pressure exerted by the surrounding soil on the pile helps it resist the load. The distribution of this soil reaction on the pile depends on three factors: the stiffness of the pile, stiffness of the soil, and stability at the ends of the pile.

To analyze such a laterally loaded pile (Davisson and Gill, 1963, as cited by Das, 2018), specific elastic solutions, indicated in Eqs. (1) and (2), are adopted to determine the deflection and moment of the pile at any given depth.

$$xz(z) = A'_X \frac{Q_g \cdot R^3}{E_p \cdot I_p} + B'_X \frac{M_g \cdot R^2}{E_p \cdot I_p}, \quad (1)$$

$$Mz(z) = A'_m \cdot Q_g \cdot R + B'_m \cdot M_g, \quad (2)$$

where A'_X, B'_X, A'_m, and B'_m denote coefficients for long piles sourced from the study conducted by Das (2018), Q_g represents the lateral load acting on the surface of the soil, M_g denotes the moment produced on the surface of the soil, I_p represents the inertia of the pile section, and E_p represents the modulus of elasticity of the pile material. Furthermore, R denotes a constant defined as in Eq. (3).

$$R = \sqrt[4]{\frac{E_p \cdot I_p}{k}} \quad (3)$$

For noncohesive soils, the reaction of the subsoil is assumed to be constant with respect to depth (Matlock and Reese, 1962, as cited in Das, 2018). The value of k appearing in Eq. (3) can be estimated using Eq. (4).

$$k_h = n_h \cdot \frac{z}{d}, \quad (4)$$

where k_h denotes the modulus of the soil reaction, n_h represents the horizontal compressibility modulus of the soil (MN/m^3), z is the depth of the pile, and d is the diameter of the pile.

2.2. Ultimate capacity of a pile group

The load capacity of a pile group is determined by Eq. (5) (Das, 2018).

$$\sum Q = Q_p + Q_s, \quad (5)$$

where Q_p represents the ultimate load capacity at the pile tip, and Q_s denotes the ultimate capacity attributed to lateral friction. The definition for Q_p is as follows:

$$Q_p = A_p . C, \quad (6)$$

where C denotes the soil resistance at the base of the pile, and A_p represents the cross-sectional area of the pile in contact with the soil.

Furthermore, the ultimate capacity attributed to lateral friction (Q_s) is defined as follows:

$$Q_s = \pi \cdot D \cdot L \cdot \sigma' \cdot \tan(\phi'), \quad (7)$$

where D denotes the pile diameter, L represents the embedment length of the pile in the soil, σ' denotes the effective pressure on the pile, and ϕ' represents the effective soil friction angle.

Moreover, the horizontal bearing capacity of piles is influenced by the properties of the pile material (such as the elastic modulus and shear strength), pile geometry (length and diameter), and loads resulting from shear and bending moments. Notably, the stiffness coefficient of a pile (η) for cohesionless soils is defined as

$$\eta = \frac{\eta_h}{EI}^{0.2}, \quad (8)$$

where EI represents the flexural strength of the pile section (MN/m^2), and n_h denotes the coefficient of variation of the soil modulus (MN/m^3).

Furthermore, the bearing capacity for flexure (M_u) is defined as follows:

$$M_U = \Upsilon_k . f . W_y, \quad (9)$$

where W_y denotes the modulus of the pile section (m^3), Υ_k represents the coefficient of reduction of the cross-sectional force, and f denotes the material strength of the pile (MPa).

Finally, the reduction coefficient of the bearing capacity ($Q_{u,red}$) allows adjustments in the magnitude of the horizontal bearing capacity, as indicated in Eq. (10).

$$Q_{u\,red} = \frac{Q_u}{\square} \gamma . Q_U, \quad (10)$$

where Q_u denotes the horizontal bearing capacity, and $\gamma . Q_u$ represents the reduction coefficient of the horizontal bearing capacity.

2.3. Winkler–Spring model

The Winkler–Spring model describes soil–structure interactions by considering the interplay among various factors such as terrain characteristics, geotechnical conditions of the site, and their influence on the responsiveness of the substructure, particularly on the distribution of stresses within the foundation (Wani et al., 2022). When using the model for describing soil–pile interactions, flexibility in design is crucial. Notably, for a pile group subjected to horizontal loads, the model is particularly useful owing to its capacity to handle large loads. Furthermore, the responses generated by the pile group structure to actual soil conditions must be analyzed. Overall, the analysis must model soil resistance as the spring force acting per unit area, separated but joined to the structure. Furthermore, the pile group must be designed to accommodate both vertical and horizontal loads, ensuring that deformations do not compromise the serviceability of the structure (Kavitha et al., 2016).

2.4. p–y curve method

The *p–y* curve is a numerical method derived from the Winkler–Spring model to analyze the interaction of soil with a pile group. This model conceptualizes soil as a series of complex, nonlinear springs, each with varying ballast coefficients along the length of the pile. Furthermore, the behavior of the soil at desired depths is represented by a series of stress–strain curves, as depicted in Figure 1. In this figure, *p* denotes the ground pressure per unit length of the pile, and *e* represents its deflection.

Matlock and Reese (1962) introduced an elastic solution leveraging *p–y* curves to evaluate the response of a pile group to lateral loads. This method computes key factors such as displacements, shear forces, bending moments, and reaction moduli of nonlinear clay soils along piles. Specifically, by varying the modulus of the horizontal reaction of the soil relative to the applied load, this analysis obtains stiffness values that ensure compatibility between the deformations of the soil and the structure.

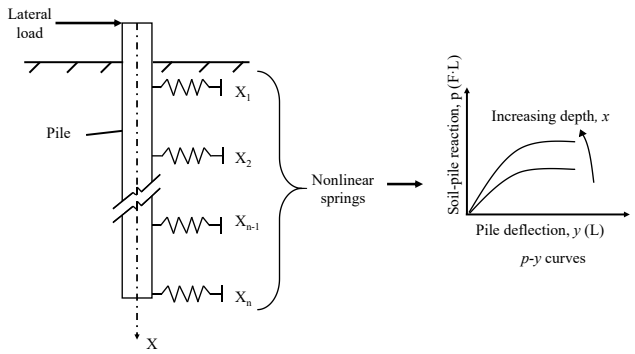

Figure 1: *p–y* curve for soils (Papavasileion, 2022).

2.5. Pile group efficiency

The efficiency of a pile group is often lower compared to that of a single pile because it is influenced by the resistance magnitudes of individual piles rather than the bearing capacity of the soil (Pérez, 2010). Furthermore, when piles are spaced at a distance of less than twice their diameter and if the pile cap is supported by the ground, the foundation can behave as a single footing, generating simultaneous vertical displacements throughout the group. Conversely, when the spacing between piles is adequate, the efficiency of the foundation is influenced by the displacement of the most heavily loaded pile. However, when incorporating the effect of pile caps, significant improvements in group efficiency are observed. Eqs. (7) and (8) provide formulas for estimating the efficiency coefficient of a pile group based on La Barré's methodology (Das, 2018).

$$\varphi = arctag\left(\frac{d}{s}\right), \tag{7}$$

$$n_g = 1 - \varphi\left(\frac{(n_x - 1)n_y + (n_y - 1)n_x}{90 n_x n_y}\right), \tag{8}$$

where n_g denotes the coefficient of the pile group; d represents the pile diameter; s denotes the center-to-center pile spacing; and n_x and n_y represent the numbers of piles along the x and y axes, respectively.

2.6. Pile group safety factor

The safety factor is critical for reducing the risk of component failure under various design, service, or extreme conditions, as well as for ensuring material reliability. The safety factor must always exceed one; specifically, the permissible stress for a design must always be less than the breaking stress. This verification methodology is widely favored owing to its clarity and simplicity because it does not require changes in load or soil parameters to obtain appropriate coefficients. Equation (9) presents the expression for the safety factor.

$$FS = \frac{x_{pas}}{x_{act}} > FS_{req}, \tag{9}$$

where FS denotes the computed safety factor, x_{pas} represents the resistance to failure, x_{act} denotes the cause of failure, and FS_{req} is the required safety factor.

3. PILE GROUP MODELING

3.1. Design procedure

Figure 2 outlines the steps for analyzing the design of a pile group, considering soil–structure interactions for more realistic outcomes. This process determines both lateral displacements and appropriate design parameters for the pile group.

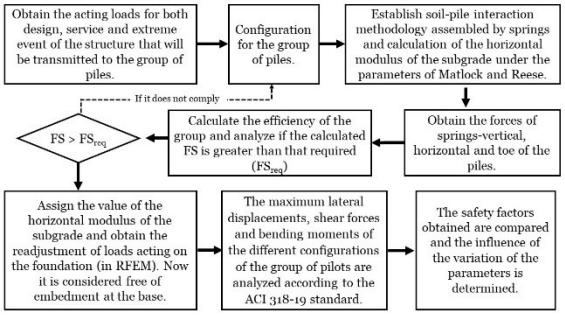

Figure 2: Computational flowchart.

The Pile Group module of Geo5® is a software tool used to solve geotechnical problems using analytical models and the limit states method. This method ensures the safety of a structure by comparing the limit load to previously established load values specified in various technical standards, such as ACI 318-19 (Geo5, 2022). To assess the interaction of the pile and soil using *p–y* curves, the pile base is considered as a floating structure.

RFEM®, a software program based on the finite element method, is designed for structural calculations and dimensional analysis of composite structures under design, service, or extreme loads. The program can be used in combination with building information modeling to model different phases of a project (Dlubal, 2020). Furthermore, RFEM® can be used to create structural, concrete, longitudinal, and reinforcing steel designs adhering to ACI 318-19 regulations, considering on-site soil conditions. Here, forces and lateral displacements are evaluated by considering soil–structure interactions, offering insights into the behaviors of individual piles within groups with varying configurations.

3.2. Case study

This study aimed to analyze the behavior of a group of piles with varying diameters under lateral loads to obtain an accurate design. This analysis considered several key factors such as soil–pile interactions, pile diameter, pile length, and separation between individual piles. Furthermore, loads transmitted through a vehicular bridge under the influence of ground pressures were evaluated (Figure 3).

The design load was determined based on the weight of the bridge structure, which covered a length of 100 m. The elements of the structure included a deck, railings, and posts, all constructed using simple type A concrete with a strength of 210 kgf/cm^2 and reinforced using structural steel with a yield limit of 4,200 kgf/cm^2. Furthermore, service loads were derived from actual loads applied by vehicles, particularly HL-93 trucks. In the four lanes, braking forces and pedestrian loads dominated. Notably, both design and service loads are specified in the Peruvian Bridges Manual, Section 2.4 (MTC, 2016).

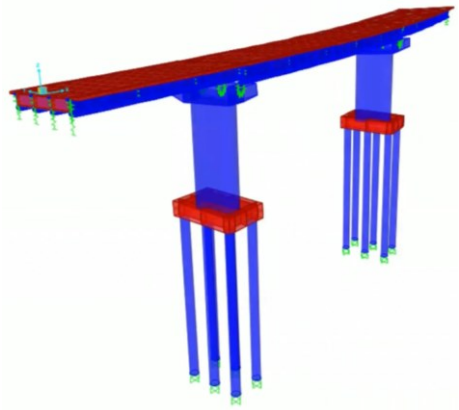

Figure 3: Case study model.

Additionally, loads resulting from extreme events, such as earthquakes, are considered. The design spectrum for Lima (Peru) is analyzed, as indicated in Table 1 and Figure 4, according to Appendix A3 of the Peruvian Bridges Manual (MTC, 2016). The derived factors help determine the seismic load acting on the pile group, which are outlined in Table 2.

Table 1: Seismic design parameters (MTC, 2016).

Seismic Design Parameters, Type B	
Maximum soil acceleration coefficient, **PGA**	0.51
Coefficient of acceleration (0.2 s), **Ss**	1.26
Coefficient of acceleration (1.0 s), **S1**	0.50
Site Coefficient, **Fpga**	1.00
Site coefficient, **Fa**	1.00
Site coefficient, **Fv**	1.00
Coefficient of acceleration, **As**	0.51
Period, **To**	0.079
Period, **Ts**	0.397
Period, **Q1**	4.00

Table 2: Loads transferred to the pile group with embedding at the base.

Load		**Design**	**Service**	**Earthquake**
Vertical Force, N	kN	12,700	9,490	11,600
Bending Moment, M_x	kN·m	8,707	5,810	6,750
Bending Moment, M_y	kN·m	5,272	3,170	4,880
Horizontal Force, H_x	kN	420	260	403
Horizontal Force, H_y	kN	172	120	137

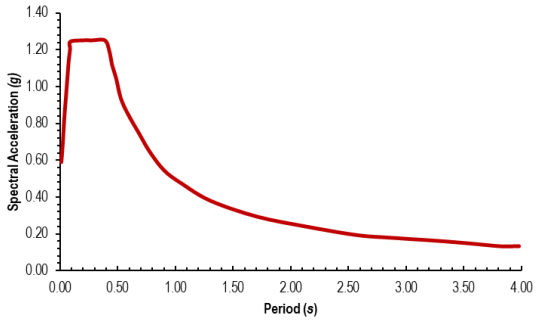

Figure 4: Seismic design spectrum (MTC, 2016).

The soil comprises two layers: the upper stratum comprises clayey sand (SC), extending to a depth of 8 m, while the second stratum comprises clayey gravel (GC), extending along the pile group. The water table is located 10 m below the soil surface. Relevant mechanical parameters are listed in Table 3.

Table 3: Soil properties.

Parameter	**SC**	**GC**
Unit weight, γ, kN/m^3	18.50	19.50
Saturated unit weight, γ_{sat}, kN/m^3	20.00	21.00
Angle of internal friction, φ_{ef}	27°	30°
Cohesion of soil, c_{ef}, kPa	8.00	6.00
Poisson's ratio, ν	0.35	0.30
Oedometric modulus, E_{oed}, kPa	12.50	67.50
Modulus of horizontal compressibility, n_h, MN/m^3	6.00	12.00
Elastic modulus, **E**, kPa	1,000	4,000
Shear modulus, **G**, kPa	370	1,540

Different configurations of the pile group are considered. The first analysis considers six piles (with diameters of 0.8, 1, and 1.2

m), arranged as illustrated in Figure 5. Each pile is embedded at a depth of 22 m below the soil surface. Individual piles are connected through a foundation slab and pile cap, which is 1.8 m thick. Specifically, the spacing between piles is designed to be no less than 1.5 times or no more than 6 times the diameter of each pile (Das, 2018). This approach is aimed at preventing instances of overlapping loads and optimizing design efficiency.

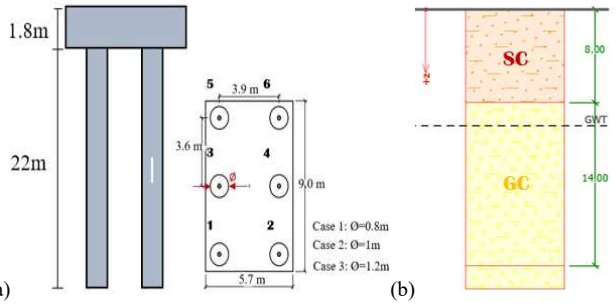

Figure 5: a) Pile group and its cross section. b) Strata of the ground.

4. RESULTS AND DISCUSSION

4.1. Winkler–Spring method

The first analysis adopted the Winkler–Spring method, which models soil as a series of springs along the pile group. Notably, this approach, valued for its simplicity, effectively evaluates soil–structure interactions by modeling the configuration of a pile group under lateral loads. First, we considered ground pressures. Furthermore, we assumed the pile tip to be a floating structure (at a depth of 22 m) rather than a resting rock. Subsequently, the vertical, horizontal, and pile tip spring forces acting per area were estimated in meganewton per square meter, reflecting the loads acting on the structure surface. However, this approach encountered limitations owing to its assumption of a constant soil stiffness along the length of the pile, which led to unrealistic results. In reality, soil pressure varies with depth, the mechanical properties of different soil strata, and water table depth.

To address these limitations, *p–y* curves were used to represent variable soil stresses. Notably, these curves can analyze changes in stiffness along each pile in different soil strata and the resulting deformations based on stress–strain relationships. When combined with the Winkler model, this methodology provides a more accurate representation of soil interactions by considering relative soil displacements resulting from stiffness variations.

Tables 4, 5, and 6 detail the vertical, horizontal, and base spring forces acting per unit area of each pile, respectively. These values were derived from Geo5, which considers soil–pile interactions and models the structure as a deformable element subjected to soil pressures.

Table 4: Vertical spring force acting per unit area of a pile (MN·m²)

Pile	0.00 m	2.20 m	4.40 m	6.60 m	8.8 m	11.00 m	13.20 m	15.40 m	17.60 m	19.80 m	22.00 m
1	3.30	3.30	3.29	3.28	10.13	19.84	19.82	19.82	19.81	19.81	19.80
2	3.29	3.29	3.28	3.28	10.12	19.81	19.80	19.79	19.79	19.78	19.78
3	2.20	2.20	2.19	2.19	6.75	13.21	13.20	13.20	13.20	13.20	13.19
4	2.19	2.19	2.19	2.19	6.73	13.19	13.18	13.18	13.18	13.17	13.17
5	3.29	3.29	3.26	3.28	10.11	19.79	19.79	19.78	19.78	19.78	19.77
6	3.28	3.28	3.28	3.28	10.09	19.76	19.75	19.75	19.74	19.74	19.74

Table 5: Vertical spring force acting per unit area of a stilt (MN·m²)

Pile	0.00–2.20 m	2.20–4.40 m	4.40–6.60 m	6.60–8.80 m	8.80–11.00 m	11.00–13.20 m	13.20–15.40 m	15.40–17.60 m	17.60–19.80 m	19.80–22.00 m
1	6.60	19.80	33.00	64.53	118.80	145.20	171.60	198.00	224.40	250.80
2	6.60	19.80	33.00	64.53	118.80	145.20	171.60	198.00	224.40	250.80
3	3.30	9.90	16.50	32.26	59.40	72.60	85.80	99.00	112.20	125.40
4	3.30	9.90	16.50	32.26	59.40	72.60	85.80	99.00	112.20	125.40
5	6.60	19.80	33.00	64.53	118.80	145.20	17.60	198.00	224.40	250.80
6	6.60	19.80	33.00	64.53	118.80	145.20	17.60	198.00	224.40	250.80

Table 6: Spring force acting per unit area at the base of each (MN·m).

Pile					
1	**2**	**3**	**4**	**5**	**6**
94.62	114.94	106.48	134.50	126.90	134.50

Table 2 summarizes the loads acting on the pile group. However, these loads are derived from an analysis that disregards soil–structure interactions and considers each pile embedded at its base. Consequently, the derived strengths and active moments are inaccurate. To address this, soil–structure interactions must be evaluated using the Winkler–Spring methodology, associated with the study of *p–y* curves. This approach allows for a more realistic assessment of the acting loads, including the vertical force, horizontal force, and bending moments, as detailed in Table 7. Thus, in this context, a structure not embedded at its base is analyzed, and pressures acting along the group of piles are considered.

Comparing Table 2 and Table 7, which present the results of the analysis considering soil–pile interactions, reveals that horizontal forces acting along the *x* and *y* directions under earthquake loads increase by 80% and 69%, respectively. This increase in attributed to the pressure exerted by the soil on the lateral area of the pile along 22 m.

Table 7. Redistribution of forces in the pile group considering soil–structure interactions.

Load	Unit	Design	Service	Earthquake
Vertical Force, N	kN	12,700	9,490	11,624
Bending Moment, M_x	kN·m	7,429	4,870	8,126
Bending Moment, M_y	kN·m	8,250	5,334	8,827
Horizontal Force, H_x	kN	691	450	730
Horizontal Force, H_y	kN	82	51	232

4.2. Efficiency (e)) and safety factor (SF)

To identify an appropriate configuration for the pile group, its efficiency must be evaluated. This parameter (e) determines the spacing between individual piles along the x-axis and y-axis to prevent overlapping loads. According to the ACI 318-19 standard, a separation of 3 to 3.5 times the pile diameter along both directions is recommended. With this spacing, an efficiency of 0.996 for the pile group was obtained, using Eqs. (7) and (8), indicating that the strength of the pile was less than the resistance of the soil.

In addition to efficiency, analyzing the safety factor is also critical. The safety factor is determined by comparing the bearing capacity of the pile—comprising the friction capacity and tip capacity of the pile—with the maximum vertical force acting on it. This comparison helps reduce the risk of component failure under varying loads. Furthermore, theoretically, the safety factor must be greater than one to ensure that the design stress is less than the breaking stress. The safety factor is calculated using Eq. (9), and the values obtained are listed in Table 8.

Table 8: Safety factors of the pile group as functions of the pile diameter.

Parameter	Case 1 Ø=0.8 m	Case 2 Ø=1 m	Case 3 Ø=1.2 m
Friction bearing capacity, Rs (kN)	4,408.36	5,976.85	7,534.37
Pile tip bearing capacity, Rb (kN)	1,603.47	2,505.42	3,607.81
Pile bearing capacity (kN)	6,011.83	8,482.27	11,142.18
Ultimate vertical force (kN)	3,634.82	3,543	3,428.62
Theoretical safety factor	2	2	2
Calculated safety factor	1.65	2.39	3.24

4.3. Forces, moments, and displacements of the pile group

Using RFEM®, a 3D model of each pile configuration was created. Here, the length of each pile was divided into 10 sections to interpolate the reaction of each pile relative to the applied loads and the force per unit area resulting from soil interactions in each section. A mesh comprising 46,535 elements was generated to analyze the normal forces, shear forces, and bending moments acting along each pile, as depicted in Figure 6 to 8.

The RFEM® program was also used to determine the lateral loads acting on the pile group, considering the most critical load for overall behavior analysis. Thus, by computing the soil reaction (k_h), the lateral load capacity was determined and compared with the maximum horizontal stresses acting on the pile group to ensure structural stability, as indicated in Table 9.

Table 9. Lateral load capacity

Parameter	Case 1 Ø = 0.8 m	Case 2 Ø = 1m	Case 3 Ø = 1.2 m
Soil reaction, Kh (MN/m³)	60–330	48–264	40–220
Maximum lateral load capacity (kN)	730.58	560.28	777.39
Lateral load (kN)	145.76	83.25	98.4
Theoretical safety factor	2	2	2
Calculated safety factor	5.01	6.73	7.9

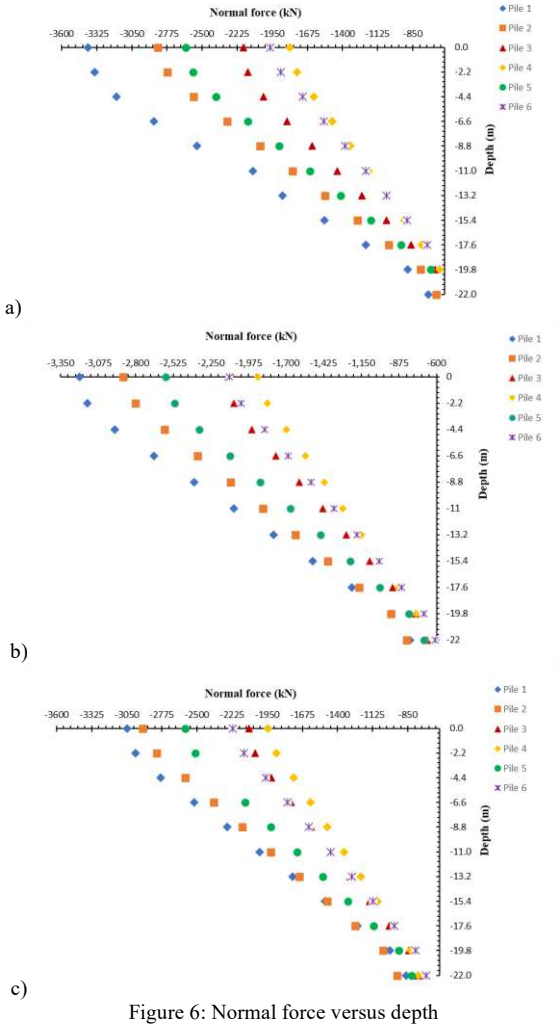

Figure 6: Normal force versus depth
(a) Ø=0.8 m, (b) Ø=1 m, and (c) Ø=1.2 m.

The configuration of the pile group significantly influenced lateral displacements. The results for the three configurations revealed that the front row piles experienced higher lateral displacements compared to the rear piles, as the lateral load decreased with increasing spacing in the configuration. Intermediate piles, in particular, exhibited lower soil–structure interactions. This is because, during a seismic event, front piles provide protection, reducing lateral displacements; however,

contour piles experience greater displacements.

Furthermore, an analysis of both lateral and global displacements was performed. The lateral displacements obtained for both axes, particularly the axis subjected to the most critical seismic load, were assessed for a pile group with a depth of 22 m and a water table at a depth of 10 m. Notably, the Winkler–Spring model and the *p*–*y* curves facilitated the analysis of the effects of lateral loads acting along the pile and at the tips of individual piles. However, each pile in the configuration is subjected to different types of loads—vertical, lateral, or bending moments—resulting in varying displacements, as illustrated in Figure 8.

Furthermore, analyzing the maximum displacements of the pile group is critical, as these are influenced by the design and service loads. The pile cap significantly influences the connection and separation between piles, impacting the overall behavior of the group.

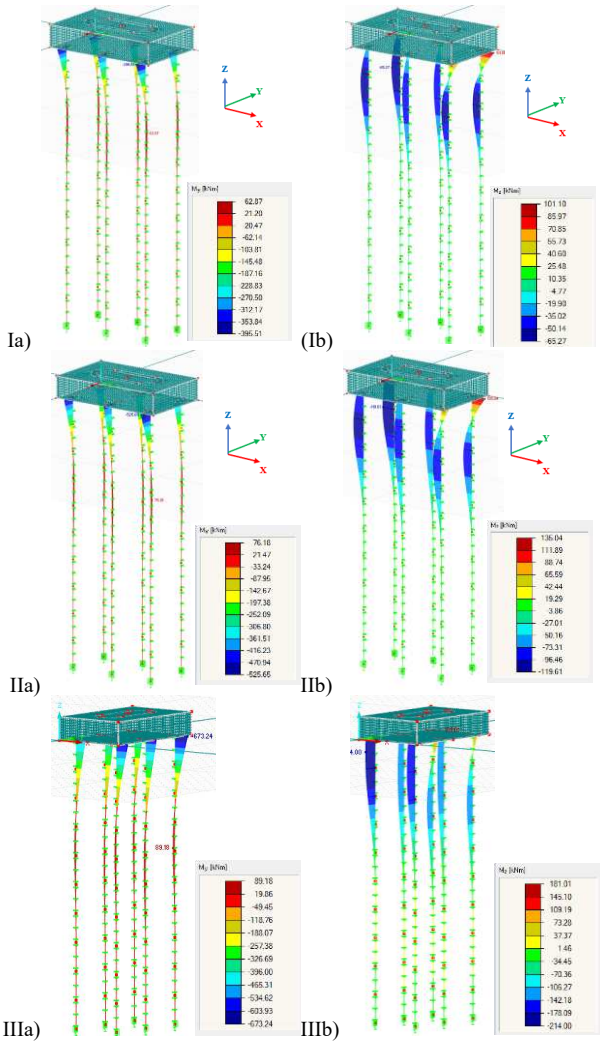

Figure 7: Shear forces (kN):
(I) Ø=0.8 m, (II) Ø=1 m; III) Ø=1.2 m; a) *y*-axis and b) *x*-axis.

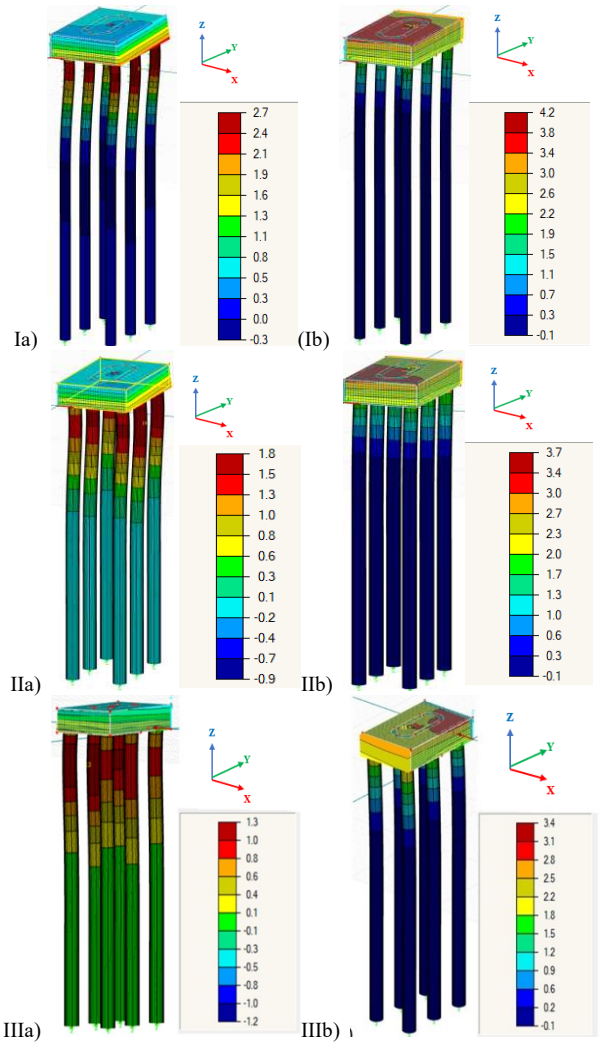

Figure 8: Bending moments (kN/m):
(I) Ø=0.8 m, (II) Ø=1 m; III) Ø=1.2 m - a) *y*-axis and b) *x*-axis.

A comparison between the three case studies highlights the variations in pile group behavior with changes in the pile diameter, particularly for piles subjected to higher or more lateral loads. First, the shear forces and bending moments acting along each axis were analyzed, and the results revealed that piles 2 and 6 were the most loaded. This is because the seismic lateral force acts in both directions. Overall, this comparison revealed that increasing the diameter of the pile improved the responsiveness of the pile group, as illustrated in Figure 9 and Figure 10. Furthermore, the forces weakened with increasing depth, becoming almost negligible at 12 m.

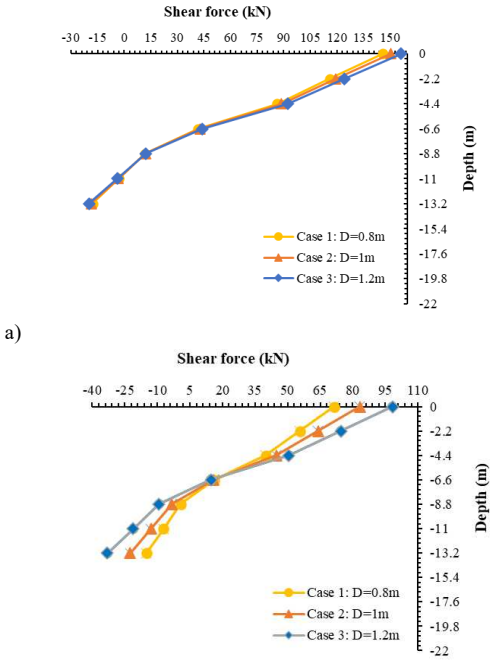

Figure 9: Shear forces versus depth: a) *x*-axis and b) *y*-axis.

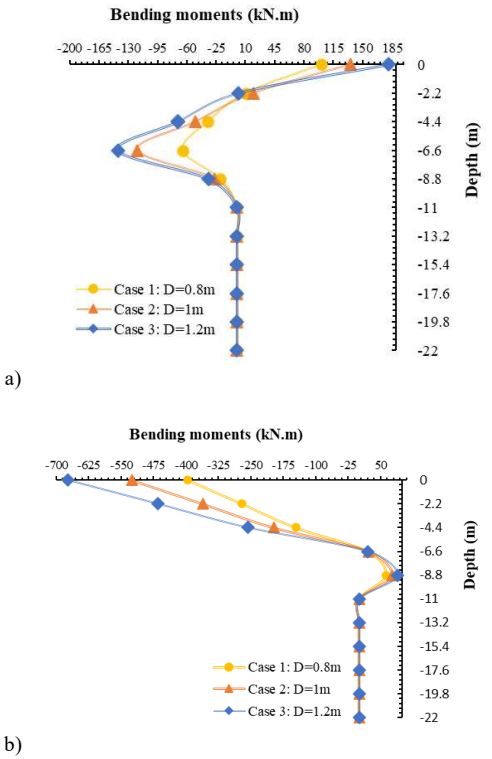

Figure 10: Bending moments versus depth: a) *x*-axis and b) *y*-axis.

Second, as the diameter of the pile group increased, lateral displacements decreased. In particular, in the most unfavorable case with a pile diameter of 0.8 m, the displacement was 4.3 mm, whereas in the most favorable case with a pile diameter of 1.2 m, the displacement was 3.4 mm, as illustrated in Figure 11. However, regarding safety factors, case 1 (Ø=0.8 m) did not comply with the design parameters, indicating that the group of piles would fail owing to compression. In contrast, cases 2 and 3 exhibited optimal safety factors, as indicated in Table 8.

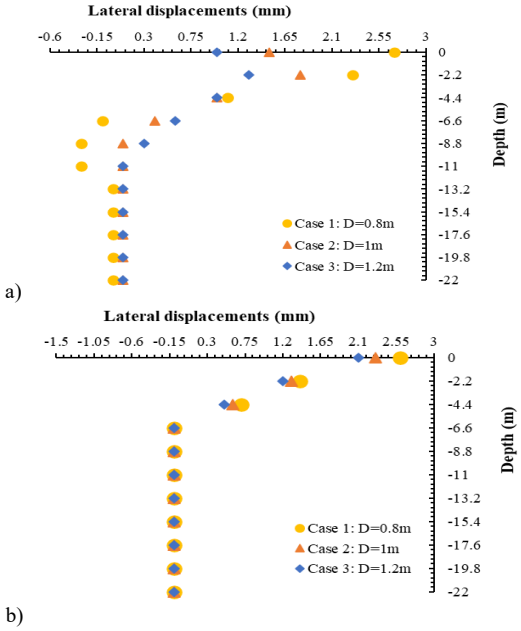

Figure 11: Lateral displacements versus depth: a) *x*-axis and b) *y*-axis.

5. CONCLUSIONS

- This study focuses on the impact of soil–structure interactions on the distribution of horizontal loads within a pile group. The method proposed by Matlock and Reese provides conservative data that facilitate accurate modeling and design by incorporating springs along the piles in relation to the soil mechanical parameters.
- The responses of piles within a group subjected to lateral loads significantly vary with their position. This underscores the importance of proper alignment of the pile group based on seismic, wind, and/or wave design spectra, considering soil mechanical conditions.
- Combining the Winkler–Spring method and *p*–*y* curves prove effective in optimizing time and resources, leading to a more accurate design. By analyzing base embedment and pile interactions at the base using RFEM®, more precise results are obtained.
- Analysis of the lateral behavior of a pile group, particularly in seismic areas, reveals that lateral loads account for 15% to 20% of the axial force. Notably, both horizontal and vertical safety factors must be determined based on soil reactions.
- Future research must focus on the behavior of pile groups on sloping terrain, exploring the variation of the soil reaction modulus with different parameters to enhance geotechnical–structural calculations and reflect real-world conditions more accurately.

ACKNOWLEDGMENTS

The authors thank the Scientific Research Institute (IDIC) of the University of Lima for their support and interest in this study.

REFERENCES

Abdrabbo, F. M., & Gaaver, K. E. (2012). Simplified analysis of laterally loaded pile groups. *Alexandria Engineering Journal*, *51*(2), 121–127. https://doi.org/10.1016/j.aej.2012.05.005

ACI Committee 318, 2019, "Building Code Requirements for Structural Concrete (ACI 318-19) and Commentary", American Concrete Institute, Farmington Hill, MI, 681 pp

Ballesteros Granados, J. A. (2018, April). 3.11. Simulación del comportamiento sísmico en grupos de pilotes usando el método de elementos finitos. In *III Congreso Internacional de Educación a Distancia y Virtual*.

Cépeda, D. (2020)" *Análisis comparativo de cimentación profunda de un centro comercial con pilotes excavados y micropilotes*". Pontificia Universidad Católica del Perú. Lima. Perú

Das, B. M. (2018). Cimentaciones con Pilotes, Fundamentos *de Ingeniería de Cimentaciones (7ma Edición, pp 535-634). Editorial. Cengage Learning. CP. 05349, Mexico, D.F.*

Dlubal. (2020). *RFEM 5 Spatial Models Calculated According to Finite Element Method User Manual*. www.dlubal.com

Geo5. (2016). User guide (edition 2017), fine civil engineering software.

Kavitha, P. E., Beena, K. S., & Narayanan, K. P. (2016). A review on soil–structure interaction analysis of laterally loaded piles. In *Innovative Infrastructure Solutions* (Vol. 1, Issue 1). Springer. https://doi.org/10.1007/s41062-016-0015-x

Kim, Y., & Jeong, S. (2011). Analysis of soil resistance on laterally loaded piles based on 3D soil-pile interaction. *Computers and Geotechnics*, *38*(2), 248–257. https://doi.org/10.1016/j.compgeo.2010.12.001.

Matlock, H and Reese, L. C. (1962). *Generalized solutions for laterally loaded piles*. Journal of Geotechnical Engineering, 86, 63-91

Ministerio de Transportes y Comunicaciones, MTC, (2018). *Manual de Puentes*. Decreto Supremo No 021-2007-MTC. Lima. Perú.

Papavasileiou, S. (2022). *Comparison of PISA and API methods for monopile under lateral loads*. Bentley Communities. https://communities.bentley.com/products/geotech-analysis/w/plaxis-soilvision-wiki/57818/comparison-of-pisa-and-api-methods-for-monopile-under-lateral-loads.

Pérez, P. (2010). *Implementación Informática para el cálculo de pilotes de hormigón In Situ según el Código Técnico de la Edificación*. Escuela Superior de Ingenieros de Sevilla. Sevilla. España.

Rollins, K. M., Lane, J. D., & Gerber, T. M. (2005). Measured and Computed Lateral Response of a Pile Group in Sand. *Journal of Geotechnical and Geoenvironmental Engineering*, *131*(1), 103–114. https://doi.org/10.1061/(asce)1090-0241(2005)131:1(103)

Stacul, S., & Squeglia, N. (2018). Analysis method for laterally loaded pile groups using an advanced modeling of reinforced concrete sections. *Materials*, *11*(2). https://doi.org/10.3390/ma11020300

Teramoto, S., Niimura, T., Akutsu, T., & Kimura, M. (2018). Evaluation of ultimate behavior of actual large-scale pile group foundation by in-situ lateral loading tests and numerical analysis. *Soils and Foundations*, *58*(4), 819–837. https://doi.org/10.1016/j.sandf.2018.03.011

Wani, F. M., Vemuri, J., Rajaram, C., & Babu R, D. V. (2022). Effect of soil structure interaction on the dynamic response of reinforced concrete structures. *Natural Hazards Research*, *2*(4), 304–315. https://doi.org/10.1016/j.nhres.2022.11.002